

# Rare $\Lambda_b \rightarrow \Lambda \ell^+ \ell^-$ decay in the two-Higgs doublet model of type III

R. F. Alnahdi, T. Barakat\*, and H. A. Alhendi

*Physics & Astronomy Department, King Saud University, P. O. Box 2455, Riyadh 11451, Saudi Arabia*

\*E-mail: tbarakat@ksu.edu.sa

Received March 17, 2017; Revised June 14, 2017; Accepted June 19, 2017; Published July 29, 2017

The rare exclusive dileptonic  $\Lambda_b \rightarrow \Lambda \ell^+ \ell^-$  ( $\ell = \mu, \tau$ ) decays are investigated in the general two-Higgs-doublet model of type III. A significant enhancement to the branching ratios, differential branching ratios, leptons forward-backward asymmetry, and the  $\Lambda$  baryon polarizations over the standard model is obtained. Measurements of these quantities will be useful for establishing the two-Higgs doublet model.

Subject Index     B53, B56, B57

## 1. Introduction

In 2012, the ATLAS and CMS experiments at CERN (Run 1) reported evidence of a particle consistent with the Higgs boson at a mass of  $\sim 125$  GeV (Refs. [1–5]). This result represents a truly fundamental discovery that is at least in the right direction to understand better the electroweak symmetry breaking via the Higgs mechanism implemented in the standard model (SM) through one scalar  $SU(2)_L$  doublet. With this discovery the large Hadron collider (LHC) completed the particle content of the SM. Nonetheless, an obvious question we are now facing is whether the discovered  $\sim 125$  GeV state corresponds to the SM Higgs boson, or whether it is just the first signal of a much richer scenario of electroweak symmetry-breaking mechanisms.

This result initiated physicists to ruminate on the different possibilities for searching for new physics beyond the SM. One of the most promising scenarios for new physics beyond the SM is an extended Higgs sector that has rich phenomenology (Ref. [6]). In this regard, the flavor-changing neutral currents (FCNC) processes, such as the electroweak penguin decays  $b \rightarrow s \ell^+ \ell^-$ , are one of these phenomena (see Ref. [7] and references therein).

Currently, the main interest is focused on the semileptonic decays of heavy hadrons  $\Lambda_b \rightarrow \Lambda \ell^+ \ell^-$  that offer cleaner probes compared to nonleptonic exclusive hadronic decays, and give valuable insight into the nature of FCNC. These decays are forbidden at the tree level in the SM, and they appear only at the one-loop level. Therefore, the study of these rare decays provides sensitive tests of many new physics models beyond the SM. The new physics effects in these decays can appear either by introducing new intermediate particles and interactions into the Wilson coefficients, or through introducing new operators into the effective Hamiltonian of such decays.

As a matter of fact, the exclusive rare  $B$  mesons described by FCNC  $b \rightarrow s \ell^+ \ell^-$  decays at the quark level, have been extensively studied with varying degrees of theoretical rigor and emphasis. In spite of the progress in the exclusive rare  $B$  mesons, so far, we have not seen any clear sign of new physics

in this  $b$  sector, but there was a tension with the SM predictions in some  $b \rightarrow s$  penguin-induced transitions. For example, the measurement by the LHCb Collaboration shows several significant deviations on angular observables related to  $B \rightarrow K^* \mu^+ \mu^-$  channels from their corresponding SM expectations (Refs. [8–21]).

Therefore, now, it is of the utmost importance to study any other such semileptonic decay modes in another sector to clarify this situation, and point out the source of these deviations. In this context, the FCNC processes in the baryonic sector receive special attention in searching for new physics effects, besides the direct searches at LHC.

Apparently, the investigations of FCNC transitions for the bottom baryonic decays can represent useful ground for finding the helicity structure of the effective Hamiltonian, which is lost in the hadronization in the meson case (Ref. [22]).

In the last few years, several theoretical works have emerged to better understand  $\Lambda_b \rightarrow \Lambda \ell^+ \ell^-$  ( $\ell = e, \mu, \tau$ ) decays in both the SM and beyond (see Refs. [23,24], and the references therein). On the experimental side, the first experimental result on the rare baryonic decay mode  $\Lambda_b \rightarrow \Lambda \mu^+ \mu^-$  has recently been reported by the CDF Collaboration at Fermilab  $\text{BR}(\Lambda_b \rightarrow \Lambda \mu^+ \mu^-) = [1.73 \pm 0.42 \text{ (stat)} \pm 0.55 \text{ (syst)}] \times 10^{-6}$  (Ref. [25]), and the LHCb Collaboration at CERN has also reported on this branching ratio mode  $\text{BR}(\Lambda_b \rightarrow \Lambda \mu^+ \mu^-) = [0.96 \pm 0.16 \text{ (stat)} \pm 0.13 \text{ (syst)} \pm 0.21 \text{ (norm)}] \times 10^{-6}$  (Ref. [26]).

Quite recently, the LHCb Collaboration has reported on both the differential branching ratio of the rare decay  $\Lambda_b \rightarrow \Lambda \mu^+ \mu^-$  and the leptons forward–backward asymmetry ( $A_{\text{FB}}$ ) in the dilepton invariant mass-squared region  $15 < q^2 < 20 \text{ GeV}^2$  as  $d\text{BR}(\Lambda_b \rightarrow \Lambda \mu^+ \mu^-)/dq^2 = (1.18^{+0.09}_{-0.08} \pm 0.03 \pm 0.27) \times 10^{-7} \text{ GeV}^{-2}$ , and  $A_{\text{FB}} = -0.05 \pm 0.09 \text{ (stat)} \pm 0.03 \text{ (syst)}$  (Ref. [27]). The errors are still quite large, but one hopes to have more new results in the near future.

Consequently, deeper understanding of such rare baryonic decays is now entering a new era. One of the motivating scenarios for new physics beyond the SM, is the two-Higgs doublet model (2HDM). Basically, the 2HDM has two complex Higgs doublets,  $\Phi_1$  and  $\Phi_2$ , rather than one, as in the SM, and the 2HDM allows FCNC at tree level, which can be avoided by imposing an ad hoc discrete symmetry. One of the possibilities for avoiding the FCNC is to couple all the quarks to  $\Phi_2$ , where  $\Phi_1$  does not couple to quarks at all, which is often known as type I. The second possibility is to couple  $\Phi_1$  to the down-type quarks, while  $\Phi_2$  couples to the up-type quarks, which is known as type II (Refs. [28,29]).

At the same time, there have been further works on a more general 2HDM without discrete symmetries as in types I and II, called type III. In this type both  $\Phi_1$  and  $\Phi_2$  couple to all quarks, and FCNC exists in type III at tree level (Refs. [30,31]). It implies that type III should be parameterized so as to suppress the tree-level FCNC couplings of the first two generations while the tree-level FCNC couplings involving the third generation can be made nonzero as long as they do not violate the existing experimental data, like,  $B^0 - \bar{B}^0$  mixing.

In this work, we shall investigate the rare exclusive  $\Lambda_b \rightarrow \Lambda \ell^+ \ell^-$  decays within 2HDM of type III. With this in mind, the structure of this work is organized as follows. In Sect. 2, we present the effective Hamiltonian for  $b \rightarrow s \ell^+ \ell^-$  transition in the 2HDM. Section 3 contains the parametrization of the matrix elements, and the derivation of the amplitude of  $\Lambda_b \rightarrow \Lambda \ell^+ \ell^-$  decay, as well as other physical observables like decay rate, leptons forward–backward asymmetry ( $A_{\text{FB}}^\ell$ ), and polarization asymmetries of the  $\Lambda$  baryon in 2HDM of type III. Section 4 is devoted to the numerical analysis of these observables. Finally, Sect. 5 contains our brief summary and concluding remarks.

## 2. The effective Hamiltonian for $b \rightarrow s\ell^+\ell^-$ transition

The baryonic  $\Lambda_b \rightarrow \Lambda\ell^+\ell^-$  ( $\ell = \mu, \tau$ ) decays at quark level are described by FCNC  $b \rightarrow s\ell^+\ell^-$  transition. The effective Hamiltonian representing these decays in both SM and 2HDM can be written in terms of a set of local operators, and takes the following basic form (Ref. [32]):

$$H_{\text{eff}} = -\frac{4G_F}{\sqrt{2}} V_{tb} V_{ts}^* \left\{ \sum_{i=1}^{10} C_i(\mu) O_i(\mu) + \sum_{i=1}^{10} C_{Qi}(\mu) Q_i(\mu) \right\}, \quad (1)$$

where  $G_F$  is the Fermi coupling constant,  $V_{tb}^* V_{ts}$  are the relevant Cabibbo–Kobayashi–Maskawa (CKM) matrix elements, and of course the terms proportional to  $V_{ub} V_{us}^*$  are ignored since  $|V_{ub} V_{us}^* / V_{tb} V_{ts}^*| < 0.02$ . Also,  $O_i(\mu)$  are the set of relevant local operators and  $C_i(\mu)$  are the Wilson coefficients that describe the short- and long-distance contributions renormalized at the energy scale  $\mu$ , which is usually taken to be the  $b$ -quark mass for  $b$ -quark decays. The additional operators  $Q_i(\mu)$  are due to the neutral Higgs bosons (NHBs) exchange diagrams, whose forms and the corresponding Wilson coefficients  $C_{Qi}(\mu)$  can be found in Ref. [33].

As we noted earlier, in the 2HDM of type III, both the doublets can couple to the up-type and down-type quarks, and without loss of generality, we can use a basis such that the first doublet produces the masses of all the gauge-bosons and fermions in the SM, whereas all the new Higgs fields originate from the second doublet. This choice permits us to write the flavor changing (FC) part of the Yukawa Lagrangian at tree level as

$$\mathcal{L}_{Y,\text{FC}}^{\text{III}} = \xi_{ij}^U \bar{Q}_{iL} \tilde{\phi}_2 U_{jR} + \xi_{ij}^D \bar{Q}_{iL} \phi_2 D_{jR} + \xi_{ij}^\ell \bar{\ell}_{iL} \phi_2 \ell_{jR} + \text{h.c.}, \quad (2)$$

where  $i, j$  are the generation indices,  $\tilde{\phi}_2 = i\sigma_2\phi_2$ .  $\xi_{ij}^{U,D,\ell}$  are in general nondiagonal coupling matrices,  $Q_{iL}$  is the left-handed fermion doublet,  $U_{iR}$  and  $D_{jR}$  are the right-handed singlets, and  $\bar{\ell}_{iL}$  and  $\ell_{jR}$  represent a left-handed SU(2) lepton doublet and a right-handed SU(2) singlet, respectively. In Eq. (2) all states are weak states, and can be transformed to the mass eigenstates by rotation.

After performing a proper rotation and diagonalization of the mass matrices for fermions and for Higgses, the flavor-changing part of the Yukawa Lagrangian is reexpressed in terms of mass eigenstates as follows (Ref. [34]):

$$\begin{aligned} \mathcal{L}_{Y,\text{FC}}^{\text{III}} = & \frac{1}{\sqrt{2}} \left[ \bar{U}_i \hat{\xi}_{ij}^U U_j + \bar{D}_i \hat{\xi}_{ij}^D D_j + \bar{\ell}_i \hat{\xi}_{ij}^\ell \ell_j \right] H^0 \\ & - \frac{i}{\sqrt{2}} \left[ \bar{U}_i \gamma_5 \hat{\xi}_{ij}^U U_j + \bar{D}_i \gamma_5 \hat{\xi}_{ij}^D D_j + \bar{\ell}_i \gamma_5 \hat{\xi}_{ij}^\ell \ell_j \right] A^0 \\ & + \bar{U}_i \left[ \hat{\xi}_{ij}^U V_{\text{CKM}} P_L - V_{\text{CKM}} \hat{\xi}_{ij}^D P_R \right] D_j H^+ + \text{h.c.}, \end{aligned} \quad (3)$$

where  $U_i, D_i, \ell_i$  are mass eigenstates of up- and down-type quarks and leptons,  $H^0, A^0$  are CP-even and CP-odd neutral Higgses, and  $H^\pm$  are charged Higgses. The  $\hat{\xi}_{ij}^{U,D,\ell}$  are the FC Yukawa quark matrices for mass eigenstates that include all the FCNC couplings,  $V_{\text{CKM}} = (V_L^U)^\dagger V_L^D$  is the usual Cabibbo–Kobayashi–Maskawa (CKM) matrix, and  $P_{L(R)} = \frac{(1 \mp \gamma_5)}{2}$  are the projection operators. Because the definition of the  $\hat{\xi}_{ij}^{U,D,\ell}$  couplings is arbitrary, in order to proceed further, in this work we adopt the Cheng–Sher ansatz (Ref. [34]),

$$\hat{\xi}_{ij}^{U,D,\ell} = \lambda_{ij} \frac{(2m_i m_j)^{1/2}}{v}, \quad (4)$$

where  $v$  is the SM vacuum expectation value (vev),  $v = 246$  GeV. This ansatz ensures that the FCNC within the first two generations are naturally suppressed by small quark masses.

In essence, from Eq. (3), it is clear that the  $b \rightarrow s\ell^+\ell^-$  transition at tree level receives contributions by exchanging neutral  $H^0$  and  $A^0$  Higgs bosons diagrams, like  $\sim \hat{\xi}_{bs} \hat{\xi}_{\mu\mu} \frac{1}{q^2 - M_{H^0(A^0)}^2} [(\bar{b}(\gamma_5)s)(\bar{\mu}(\gamma_5)\mu)] H^0(A^0)$ . In the following, we assume that the neutral Higgs boson masses are heavy enough to avoid such contributions to  $B_s \rightarrow \mu^+\mu^-$  decay and similar related processes (see Ref. [5], and references therein). Thus, from the above discussion it is clear that we can safely neglect the NHBs exchange diagrams, and the transition  $b \rightarrow s\ell^+\ell^-$  receives contributions only at loop level by exchanging the  $W^\pm, Z, \gamma$ , and charged Higgs boson fields. Interestingly, the charged Higgs boson exchange diagrams do not produce new operators for the  $b \rightarrow s\ell^+\ell^-$  transition, and only modify the value of the SM Wilson coefficients (Ref. [35]).

Consequently, the operators responsible for the dileptonic  $\Lambda_b \rightarrow \Lambda\ell^+\ell^-$  decay are only  $O_7, O_9, O_{10}$ , and the corresponding effective Hamiltonian in the SM and 2HDM for the  $b \rightarrow s\ell^+\ell^-$  transition can be written as

$$H_{\text{eff}}(b \rightarrow s\ell^+\ell^-) = \frac{G_F \alpha_{\text{em}}}{2\sqrt{2}\pi} V_{tb} V_{ts}^* \left\{ C_9^{2\text{HDM}}(\mu) \bar{s}\gamma_\mu(1-\gamma_5)b(\bar{\ell}\gamma^\mu\ell) + C_{10}^{2\text{HDM}}(\mu) \bar{s}\gamma_\mu(1-\gamma_5)b(\bar{\ell}\gamma^\mu\gamma_5\ell) - 2m_b C_7^{2\text{HDM}}(\mu) \bar{s}i\sigma_{\mu\nu} \frac{q^\nu}{q^2}(1+\gamma_5)b(\bar{\ell}\gamma^\mu\ell) \right\}, \quad (5)$$

with (Ref. [35])

$$C_7^{2\text{HDM}}(\mu) = C_7^{\text{SM}}(\mu) + |\lambda_{tt}|^2 \left( \frac{y(7-5y-8y^2)}{72(y-1)^3} + \frac{y^2(3y-2)}{12(y-1)^4} \ln y \right) + |\lambda_{tt}\lambda_{bb}| e^{i\theta} \left( \frac{y(3-5y)}{12(y-1)^2} + \frac{y(3y-2)}{6(y-1)^3} \ln y \right), \quad (6)$$

$$C_9^{2\text{HDM}}(\mu) = C_9^{\text{SM}}(\mu) + |\lambda_{tt}|^2 \left[ \frac{1-4\sin^2\theta_W}{\sin^2\theta_W} \frac{xy}{8} \left( \frac{1}{y-1} - \frac{1}{(y-1)^2} \ln y \right) - y \left( \frac{47y^2-79y+38}{108(y-1)^3} - \frac{3y^3-6y+4}{18(y-1)^4} \ln y \right) \right], \quad (7)$$

$$C_{10}^{2\text{HDM}}(\mu) = C_{10}^{\text{SM}}(\mu) + |\lambda_{tt}|^2 \frac{1}{\sin^2\theta_W} \frac{xy}{8} \left( -\frac{1}{y-1} + \frac{1}{(y-1)^2} \ln y \right), \quad (8)$$

where  $x = \frac{m_t^2}{m_W^2}$  and  $y = \frac{m_t^2}{m_{H^\pm}^2}$ . The calculations of the Wilson coefficients  $C_7^{\text{SM}}(\mu)$ ,  $C_9^{\text{SM}}(\mu)$ , and  $C_{10}^{\text{SM}}(\mu)$  are performed at next-to-leading order, and their explicit expressions at the energy scale  $\mu = m_b$  are given in Ref. [36], while their numerical values are listed in Table 1.

In the 2HDM, the free parameters are the mass of the charged Higgs boson  $m_{H^\pm}$ , and the coefficients  $\lambda_{tt}, \lambda_{bb}$ . The coefficients  $\lambda_{tt}$  and  $\lambda_{bb}$  for type III of 2HDM are complex parameters of order  $\mathcal{O}(1)$ ,

**Table 1.** The numerical values of the Wilson coefficients at  $\mu = m_b$  scale within the SM (Ref. [36]).

$C_1$	$C_2$	$C_3$	$C_4$	$C_5$	$C_6$	$C_7^{\text{SM}}$	$C_9^{\text{SM}}$	$C_{10}^{\text{SM}}$
-0.248	1.107	0.011	-0.026	0.007	-0.031	-0.313	4.344	-4.669

so that  $\lambda_{tt}\lambda_{bb} \equiv |\lambda_{tt}\lambda_{bb}|e^{i\theta}$ , where  $\theta$  is the only single CP phase of the vacuum in this version. In this way,  $\lambda_{ij}$  allow the charged Higgs boson to interfere destructively or constructively with the SM contributions.

Additionally, the Wilson coefficient  $C_9^{\text{2HDM}}(\mu)$  receives long-distance contributions coming from the charmonium resonances  $J/\psi$ ,  $\psi'$ , ..., and is replaced by an effective coefficient  $C_9^{\text{eff}}(\mu)$  (Ref. [36]):

$$C_9^{\text{eff}}(\mu) = C_9^{\text{2HDM}}(\mu)\eta(s') + Y_{\text{SD}}(n, s') + Y_{\text{LD}}(n, s'), \quad (9)$$

where the parameters  $n$  and  $s'$  are defined as  $n = m_c/m_b$ ,  $s' = q^2/m_b^2$ , whereas,  $\eta(s') = 1 + \frac{\alpha_s(\mu)}{\pi} \omega(s')$ , with

$$\begin{aligned} \omega(s') = & -\frac{2}{9}\pi^2 - \frac{4}{3}\text{Li}_2(s') - \frac{2}{3}\ln s' \ln(1-s') - \frac{5+4s'}{3(1+2s')}\ln(1-s') \\ & - \frac{2s'(1+s')(1-2s')}{3(1-s')^2(1+2s')}\ln s' + \frac{5+9s'-6s'^2}{6(1-s')(1+2s')}, \end{aligned} \quad (10)$$

$$\begin{aligned} Y_{\text{SD}}(n, s') = & h(n, s')[3C_1(\mu) + C_2(\mu) + 3C_3(\mu) + C_4(\mu) + 3C_5(\mu) + C_6(\mu)] \\ & - \frac{1}{2}h(1, s')[4C_3(\mu) + 4C_4(\mu) + 3C_5(\mu) + C_6(\mu)] - \frac{1}{2}h(0, s')[C_3(\mu) + 3C_4(\mu)] \\ & + \frac{2}{9}[3C_3(\mu) + C_4(\mu) + 3C_5(\mu) + C_6(\mu)], \end{aligned} \quad (11)$$

$$\begin{aligned} Y_{\text{LD}}(n, s') = & \frac{3}{\alpha_{\text{em}}^2}[3C_1(\mu) + C_2(\mu) + 3C_3(\mu) + C_4(\mu) + 3C_5(\mu) + C_6(\mu)] \\ & \times \sum_{j=\psi, \psi'} k_j \frac{\pi \Gamma(j \rightarrow l^+l^-) M_j}{q^2 - M_j^2 + iM_j \Gamma_j^{\text{tot}}}, \end{aligned} \quad (12)$$

where

$$\begin{aligned} h(n, s') = & -\frac{8}{9}\ln n + \frac{8}{27} + \frac{4}{9}x - \frac{2}{9}(2+x)|1-x|^{1/2} \begin{cases} \ln \left| \frac{(1-x)^{1/2}+1}{(1-x)^{1/2}-1} \right| - i\pi & \text{for } x \equiv 4n^2/s' < 1, \\ 2 \arctan \frac{1}{(x-1)^{1/2}} & \text{for } x \equiv 4n^2/s' > 1, \end{cases} \\ h(0, s') = & \frac{8}{27} - \frac{8}{9}\ln \frac{m_b}{\mu} - \frac{4}{9}\ln s' + \frac{4}{9}i\pi, \end{aligned} \quad (13)$$

and  $k_j$  are phenomenological parameters introduced to compensate for vector meson dominance and the factorization approximation, and are taken to be  $\kappa \cong 1.0$  and  $\kappa \cong 2.0$  for the lowest resonances  $J/\psi$  and  $\psi'$  respectively, and  $M_j$ ,  $\Gamma_j^{\text{tot}}$ , and  $\Gamma(j \rightarrow l^+l^-)$  are the masses, total widths, and partial widths of the resonances, respectively.

Further, the Wilson coefficient  $C_7^{\text{2HDM}}(\mu)$  receives other nonfactorizable effects coming from the charm loop that can bring further corrections to the radiative  $b \rightarrow s\gamma$  transition (Ref. [37]):

$$C_7^{\text{eff}}(\mu) = C_7^{\text{2HDM}}(\mu) + C_{b \rightarrow s\gamma}(\mu), \quad (14)$$

while the Wilson coefficient  $C_{10}^{\text{2HDM}}$  does not change under the renormalization procedure mentioned above, and so is independent of the energy scale, so we will let  $C_{10}^{\text{eff}}(\mu) \equiv C_{10}^{\text{2HDM}}(m_W)$ .

In terms of the above criteria, the effective Hamiltonian of Eq. (5) in the 2HDM can be rewritten as

$$H_{\text{eff}}(b \rightarrow s\ell^+\ell^-) = \frac{G_F \alpha_{\text{em}}}{2\sqrt{2}\pi} V_{tb} V_{ts}^* \left\{ C_9^{\text{eff}}(\mu) \bar{s}\gamma_\mu (1 - \gamma_5) b(\bar{\ell}\gamma^\mu \ell) + C_{10}^{\text{eff}}(\mu) \bar{s}\gamma_\mu (1 - \gamma_5) b(\bar{\ell}\gamma^\mu \gamma_5 \ell) \right. \\ \left. - 2m_b C_7^{\text{eff}}(\mu) \bar{s}i\sigma_{\mu\nu} \frac{q^\nu}{q^2} (1 + \gamma_5) b(\bar{\ell}\gamma^\mu \ell) \right\}, \quad (15)$$

where  $q$  is the sum of 4 momenta of  $\ell^+$  and  $\ell^-$ ,  $\alpha_{\text{em}}$  is the fine structure constant, and  $C_7^{\text{eff}}(\mu)$ ,  $C_9^{\text{eff}}(\mu)$ , and  $C_{10}^{\text{eff}}(\mu)$  are renamed to be the modified Wilson coefficients representing the different interactions including both the SM and 2HDM contributions.

### 3. Phenomenological observables of $\Lambda_b \rightarrow \Lambda \ell^+ \ell^-$ decay in the 2HDM

#### 3.1. Matrix elements

To get the matrix elements for  $\Lambda_b \rightarrow \Lambda \ell^+ \ell^-$  decay, it is necessary to sandwich the effective Hamiltonian of  $b \rightarrow s\ell^+\ell^-$  between the initial and final baryon states. Equation (15) has 4 basic hadronic matrix elements:  $\langle \Lambda | \bar{s}\gamma_\mu b | \Lambda_b \rangle$ ,  $\langle \Lambda | \bar{s}\gamma_\mu \gamma_5 b | \Lambda_b \rangle$ ,  $\langle \Lambda | \bar{s}i\sigma_{\mu\nu} q^\nu b | \Lambda_b \rangle$ , and  $\langle \Lambda | \bar{s}i\sigma_{\mu\nu} \gamma_5 q^\nu b | \Lambda_b \rangle$ . These hadronic matrix elements in terms of a set of unknown form factors are parameterized as (Ref. [38])

$$\langle \Lambda | \bar{s}\gamma_\mu b | \Lambda_b \rangle = \bar{u}_\Lambda \left[ f_1(q^2) \gamma_\mu + i f_2(q^2) \sigma_{\mu\nu} q^\nu + f_3(q^2) q_\mu \right] u_{\Lambda_b}, \\ \langle \Lambda | \bar{s}\gamma_\mu \gamma_5 b | \Lambda_b \rangle = \bar{u}_\Lambda \left[ g_1(q^2) \gamma_\mu \gamma_5 + i g_2(q^2) \sigma_{\mu\nu} \gamma_5 q^\nu + g_3(q^2) \gamma_5 q_\mu \right] u_{\Lambda_b}, \\ \langle \Lambda | \bar{s}i\sigma_{\mu\nu} q^\nu b | \Lambda_b \rangle = \bar{u}_\Lambda \left[ f_1^T(q^2) \gamma_\mu + i f_2^T(q^2) \sigma_{\mu\nu} q^\nu + f_3^T(q^2) q_\mu \right] u_{\Lambda_b}, \\ \langle \Lambda | \bar{s}i\sigma_{\mu\nu} \gamma_5 q^\nu b | \Lambda_b \rangle = \bar{u}_\Lambda \left[ g_1^T(q^2) \gamma_\mu \gamma_5 + i g_2^T(q^2) \sigma_{\mu\nu} \gamma_5 q^\nu + g_3^T(q^2) \gamma_5 q_\mu \right] u_{\Lambda_b}. \quad (16)$$

Currently, there are some studies in the literature on  $\Lambda_b \rightarrow \Lambda$  transition form factors such as heavy quark effective theory (HQET) (Ref. [39]), lattice QCD calculations (Ref. [40]), the light-cone sum rules approach (Ref. [41]), the perturbative QCD approach (Ref. [42]), the QCD sum rule approach (Ref. [43]), and the Bethe–Salpeter equation approach (Ref. [44]). In the present work, based on lattice QCD calculations (Ref. [40]), the form factors  $f_1(q^2), f_2(q^2), f_3(q^2), g_1(q^2), g_2(q^2), g_3(q^2), f_1^T(q^2), f_2^T(q^2), f_3^T(q^2), g_1^T(q^2), g_2^T(q^2)$ , and  $g_3^T(q^2)$ , introduced above in Eq. (16), are related to the helicity form factors of Ref. [40] as follows:

$$f_+(q^2) = f_1(q^2) - \frac{q^2}{(m_{\Lambda_b} + m_\Lambda)} f_2(q^2), \quad (17)$$

$$f_\perp(q^2) = f_1(q^2) - (m_{\Lambda_b} + m_\Lambda) f_2(q^2), \quad (18)$$

$$f_0(q^2) = f_1(q^2) + \frac{q^2}{(m_{\Lambda_b} - m_\Lambda)} f_3(q^2), \quad (19)$$

$$g_+(q^2) = g_1(q^2) + \frac{q^2}{(m_{\Lambda_b} - m_\Lambda)} g_2(q^2), \quad (20)$$

$$g_{\perp}(q^2) = g_1(q^2) + (m_{\Lambda_b} - m_{\Lambda})g_2(q^2), \quad (21)$$

$$g_0(q^2) = g_1(q^2) - \frac{q^2}{(m_{\Lambda_b} + m_{\Lambda})}g_3(q^2), \quad (22)$$

$$h_{+}(q^2) = f_2^T(q^2) + \frac{(m_{\Lambda_b} + m_{\Lambda})}{(m_{\Lambda_b} - m_{\Lambda})}f_3^T(q^2), \quad (23)$$

$$h_{\perp}(q^2) = f_2^T(q^2) - \frac{f_1^T(q^2)}{(m_{\Lambda_b} + m_{\Lambda})}, \quad (24)$$

$$\tilde{h}_{+}(q^2) = g_2^T(q^2) - g_3^T(q^2), \quad (25)$$

$$\tilde{h}_{\perp}(q^2) = g_2^T(q^2) + \frac{g_1^T(q^2)}{(m_{\Lambda_b} - m_{\Lambda})}. \quad (26)$$

The above helicity form factors  $f_{+}(q^2)$ ,  $f_{\perp}(q^2)$ ,  $f_0(q^2)$ ,  $g_{+}(q^2)$ ,  $g_{\perp}(q^2)$ ,  $g_0(q^2)$ ,  $h_{+}(q^2)$ ,  $h_{\perp}(q^2)$ ,  $\tilde{h}_{+}(q^2)$ , and  $\tilde{h}_{\perp}(q^2)$  are parameterized based on lattice QCD calculations in the following way (Ref. [40]):

$$f(q^2) = \frac{1}{1 - q^2/(m_{\text{pole}}^f)^2} [d_0^f + d_1^f \kappa(q^2)], \quad (27)$$

where

$$\kappa(q^2) = \frac{(t_{+} - q^2)^{1/2} - (t_{+} - t_0)^{1/2}}{(t_{+} - q^2)^{1/2} + (t_{+} - t_0)^{1/2}}. \quad (28)$$

Here,  $t_0 = q_{\max}^2 = (m_{\Lambda_b} - m_{\Lambda})^2$ ,  $t_{+} = (m_B + m_K)^2$ ,  $m_B = 5.279$  GeV,  $m_K = 0.494$  GeV, and the values of the parameters  $d_0^f$ ,  $d_1^f$ , and  $m_{\text{pole}}^f$  to the first-order fit are collected in Table 2.

**Table 2.** The central values for the form factors parameters  $d_0^f$  and  $d_1^f$  involved in the fit of Eq. (27) using the lattice QCD approach (Ref. [40]). Values of the pole masses  $m_{\text{pole}}^*$  are from the Particle Data Group (Ref. [52]), while  $m_{\text{pole}}$  masses were taken from the lattice QCD calculations (Ref. [53]).

Parameter	Value	$m_{\text{pole}}^f$ (GeV)	Parameter	Value	$m_{\text{pole}}$ (GeV)
$d_0^{f+}$	0.4221	5.416*	$a_1^{g_0}$	-1.0290	5.367*
$d_1^{f+}$	-1.1386	5.416*	$a_1^{g_{\perp}}$	-1.1357	5.750
$d_0^{f0}$	0.3725	5.711	$a_0^{h_{+}}$	0.4960	5.416*
$d_1^{f0}$	-0.9389	5.711	$a_1^{h_{+}}$	-1.1275	5.416*
$d_0^{f\perp}$	0.5182	5.416*	$a_0^{h_{\perp}}$	0.3876	5.416*
$d_1^{f\perp}$	-1.3495	5.416*	$a_1^{h_{\perp}}$	-0.9623	5.416*
$a_0^{g_{\perp}, g_{+}}$	0.3563	5.750	$a_0^{\tilde{h}_{\perp}, \tilde{h}_{+}}$	0.3403	5.750
$a_1^{g_{+}}$	-1.0612	5.750	$a_1^{\tilde{h}_{+}}$	-0.7697	5.750
$a_0^{g_0}$	0.4028	5.367*	$a_1^{\tilde{h}_{\perp}}$	-0.8008	5.750

With the above definitions of transition matrix elements, and the form factors, we get the effective amplitude for  $\Lambda_b \rightarrow \Lambda \ell^+ \ell^-$  decay:

$$\begin{aligned} \mathcal{M}(\Lambda_b \rightarrow \Lambda \ell^+ \ell^-) = & \frac{G_F \alpha_{\text{em}}}{4\sqrt{2}\pi} V_{tb} V_{ts}^* \left\{ \bar{\ell} \gamma^\mu \ell \bar{u}_\Lambda \left[ A_1 \gamma_\mu (1 + \gamma_5) + B_1 \gamma_\mu (1 - \gamma_5) \right. \right. \\ & + i \sigma_{\mu\nu} q^\nu \left( A_2 (1 + \gamma_5) + B_2 (1 - \gamma_5) \right) \\ & + q_\mu \left( A_3 (1 + \gamma_5) + B_3 (1 - \gamma_5) \right) \left. \right] u_{\Lambda_b} \\ & + \bar{\ell} \gamma^\mu \gamma_5 \ell \bar{u}_\Lambda \left[ D_1 \gamma_\mu (1 + \gamma_5) + E_1 \gamma_\mu (1 - \gamma_5) \right. \\ & + i \sigma_{\mu\nu} q^\nu \left( D_2 (1 + \gamma_5) + E_2 (1 - \gamma_5) \right) \\ & \left. \left. + q_\mu \left( D_3 (1 + \gamma_5) + E_3 (1 - \gamma_5) \right) \right] u_{\Lambda_b} \right\}, \end{aligned} \quad (29)$$

where the various functions  $A_i$ ,  $B_i$ ,  $D_j$ , and  $E_j$  ( $i, j = 1, 2, 3$ ) are defined as

$$\begin{aligned} A_i &= C_9^{\text{eff}} (f_i - g_i) - \frac{2m_b C_7^{\text{eff}}}{q^2} (f_i^T + g_i^T), \\ B_i &= C_9^{\text{eff}} (f_i + g_i) - \frac{2m_b C_7^{\text{eff}}}{q^2} (f_i^T - g_i^T), \\ D_j &= C_{10}^{\text{eff}} (f_j - g_j), \quad E_j = C_{10}^{\text{eff}} (f_j + g_j). \end{aligned} \quad (30)$$

### 3.2. The differential decay rate for $\Lambda_b \rightarrow \Lambda \ell^+ \ell^-$

The differential decay rate of  $\Lambda_b \rightarrow \Lambda \ell^+ \ell^-$  is given by

$$d\Gamma = \frac{1}{4m_{\Lambda_b}} \left( \prod_f \frac{d^3 p_f}{(2\pi)^3 2E_f} \right) (2\pi)^4 \delta^4 \left( p_{\Lambda_b} - \sum_f p_f \right) |\overline{\mathcal{M}}|^2. \quad (31)$$

Here,  $|\overline{\mathcal{M}}|^2$  is the squared amplitude averaged over the initial polarization and summed over the final polarizations. After lengthy, but straightforward calculations, one can get the double differential decay rate in terms of the various form factors in the 2HDM:

$$\frac{d^2 \Gamma(\hat{s}, z)}{d\hat{s} dz} = \frac{G_F^2 \alpha_{\text{em}}^2}{2^{14} \pi^5} |V_{tb} V_{ts}^*|^2 m_{\Lambda_b} v_\ell \lambda^{1/2}(1, r, \hat{s}) T(\hat{s}, z), \quad (32)$$

where  $\hat{s} = q^2/m_{\Lambda_b}^2$ ,  $z = \cos \theta$  is the angle between  $p_{\Lambda_b}$  and  $p_+$  in the center of mass frame of the  $\ell^+ \ell^-$  pair,  $v_\ell = (1 - 4m_{\Lambda_b} m_\ell^2/\hat{s})^{1/2}$ ,  $\lambda(1, r, \hat{s}) = 1 + r^2 + \hat{s}^2 - 2r - 2\hat{s} - 2r\hat{s}$  is the usual triangle function. The function  $T(\hat{s}, z)$  is given by

$$T(\hat{s}, z) = T_0(\hat{s}) + z T_1(\hat{s}) + z^2 T_2(\hat{s}), \quad (33)$$

with

$$\begin{aligned}
T_0(\hat{s}) = & 32m_\ell^2 m_{\Lambda_b}^2 \hat{s}(1+r-\hat{s})(|D_3|^2 + |E_3|^2) \\
& + 64m_\ell^2 m_{\Lambda_b}^3 (1-r-\hat{s}) \operatorname{Re}(D_1^* E_3 + D_3 E_1^*) + 64m_{\Lambda_b}^2 \sqrt{r}(6m_\ell^2 - \hat{s}m_{\Lambda_b}^2) \operatorname{Re}(D_1^* E_1) \\
& + 64m_\ell^2 m_{\Lambda_b}^3 \sqrt{r} \left( 2m_{\Lambda_b} \hat{s} \operatorname{Re}(D_3^* E_3) + (1-r+\hat{s}) \operatorname{Re}(D_1^* D_3 + E_1^* E_3) \right) \\
& + 32m_{\Lambda_b}^2 (2m_\ell^2 + m_{\Lambda_b}^2 \hat{s}) \left( (1-r+\hat{s})m_{\Lambda_b} \sqrt{r} \operatorname{Re}(A_1^* A_2 + B_1^* B_2) \right. \\
& - m_{\Lambda_b} (1-r-\hat{s}) \operatorname{Re}(A_1^* B_2 + A_2^* B_1) - 2\sqrt{r} \left[ \operatorname{Re}(A_1^* B_1) + m_{\Lambda_b}^2 \hat{s} \operatorname{Re}(A_2^* B_2) \right] \Big) \\
& + 8m_{\Lambda_b}^2 \left( 4m_\ell^2 (1+r-\hat{s}) + m_{\Lambda_b}^2 [(1-r)^2 - \hat{s}^2] \right) (|A_1|^2 + |B_1|^2) \\
& + 8m_{\Lambda_b}^4 \left( 4m_\ell^2 [\lambda + (1+r-\hat{s})\hat{s}] + m_{\Lambda_b}^2 \hat{s}[(1-r)^2 - \hat{s}^2] \right) (|A_2|^2 + |B_2|^2) \\
& - 8m_{\Lambda_b}^2 \left( 4m_\ell^2 (1+r-\hat{s}) - m_{\Lambda_b}^2 [(1-r)^2 - \hat{s}^2] \right) (|D_1|^2 + |E_1|^2) \\
& + 8m_{\Lambda_b}^5 \hat{s} v_\ell^2 \left( -8m_{\Lambda_b} \hat{s} \sqrt{r} \operatorname{Re}(D_2^* E_2) + 4(1-r+\hat{s}) \sqrt{r} \operatorname{Re}(D_1^* D_2 + E_1^* E_2) \right. \\
& \left. - 4(1-r-\hat{s}) \operatorname{Re}(D_1^* E_2 + D_2^* E_1) + m_{\Lambda_b} [(1-r)^2 - \hat{s}^2] \left[ |D_2|^2 + |E_2|^2 \right] \right), \quad (34)
\end{aligned}$$

$$\begin{aligned}
T_1(\hat{s}) = & -16m_{\Lambda_b}^4 \hat{s} v_\ell (\lambda(1,r,\hat{s}))^{1/2} \left\{ 2 \operatorname{Re}(A_1^* D_1) - 2 \operatorname{Re}(B_1^* E_1) \right. \\
& + 2m_{\Lambda_b} \operatorname{Re}(B_1^* D_2 - B_2^* D_1 + A_2^* E_1 - A_1^* E_2) \Big\} \\
& + 32m_{\Lambda_b}^5 \hat{s} v_\ell (\lambda(1,r,\hat{s}))^{1/2} \left\{ m_{\Lambda_b} (1-r) \operatorname{Re}(A_2^* D_2 - B_2^* E_2) \right. \\
& \left. + \sqrt{r} \operatorname{Re}(A_2^* D_1 + A_1^* D_2 - B_2^* E_1 - B_1^* E_2) \right\}, \quad (35)
\end{aligned}$$

and

$$\begin{aligned}
T_2(\hat{s}) = & 8m_{\Lambda_b}^6 v_\ell^2 \lambda(1,r,\hat{s}) \hat{s} \left( (|A_2|^2 + |B_2|^2 + |D_2|^2 + |E_2|^2) \right. \\
& \left. - 8m_{\Lambda_b}^4 v_\ell^2 \lambda(1,r,\hat{s}) (|A_1|^2 + |B_1|^2 + |D_1|^2 + |E_1|^2) \right). \quad (36)
\end{aligned}$$

The unpolarized differential decay rate of  $\Lambda_b \rightarrow \Lambda \ell^+ \ell^-$  can be obtained from Eq. (32) by integrating out the angular-dependent variable  $z$  which, in turn, yields

$$\left( \frac{d\Gamma(\hat{s})}{d\hat{s}} \right)_0 = \frac{G_F^2 \alpha_{\text{em}}^2 m_{\Lambda_b}}{2^{13} \pi^5} |V_{tb} V_{ts}^*|^2 v_\ell \lambda^{1/2}(1,r,\hat{s}) \left[ T_0(\hat{s}) + \frac{1}{3} T_2(\hat{s}) \right]. \quad (37)$$

### 3.3. Leptons forward–backward asymmetry of $\Lambda_b \rightarrow \Lambda \ell^+ \ell^-$

Another useful observable to look for new physics effects in  $\Lambda_b \rightarrow \Lambda \ell^+ \ell^-$  decay is the leptons forward–backward asymmetry ( $A_{\text{FB}}$ ). Since  $A_{\text{FB}}$  depends on the chirality of the hadronic and leptonic currents, this observable is therefore very sensitive to new physics beyond the SM through shifting its zero value position. To calculate the leptons forward–backward asymmetry, we consider the double differential decay rate formula for the process  $\Lambda_b \rightarrow \Lambda \ell^+ \ell^-$  defined in Eq. (32).

The normalized leptons forward–backward asymmetry is defined as

$$A_{\text{FB}}(\hat{s}) = \frac{\int_0^1 \frac{d\Gamma}{d\hat{s} dz} dz - \int_{-1}^0 \frac{d\Gamma}{d\hat{s} dz} dz}{\int_0^1 \frac{d\Gamma}{d\hat{s} dz} dz + \int_{-1}^0 \frac{d\Gamma}{d\hat{s} dz} dz}. \quad (38)$$

Following the same procedure as for the differential decay rate, one can easily get the expression for the leptons forward–backward asymmetry:

$$A_{\text{FB}}(\hat{s}) = \frac{T_1(\hat{s})}{2(T_0(\hat{s}) + T_2(\hat{s})/3)}. \quad (39)$$

### 3.4. $\Lambda_b \rightarrow \Lambda \ell^+ \ell^-$ decay with polarized $\Lambda$

Now let us consider the case when the final  $\Lambda$  baryon is polarized. As we already noted, unlike mesonic decays, the baryonic decays could keep the helicity structure of their interactions. The importance of the polarization of baryons in general is coming in due to their right-handed couplings, which are suppressed in the SM, and they include different combinations of structures within the Wilson coefficients  $C_7^{\text{eff}}(\mu)$ ,  $C_9^{\text{eff}}(\mu)$ , and  $C_{10}^{\text{eff}}(\mu)$ . For this reason, the baryonic decays are considered to be one of the promising tools to search for new physics beyond the SM.

Here, we present the formulas for the polarized differential decay rates of  $\Lambda_b \rightarrow \Lambda \ell^+ \ell^-$ . In the calculations, we have included the lepton masses, and we define a 4-dimensional spin vector for the polarized  $\Lambda$  baryon in terms of a unit vector,  $\hat{\xi}$ , along the direction of  $\Lambda$  spin in its rest frame as

$$s_\mu = \left( \frac{\vec{p}_\Lambda \cdot \hat{\xi}}{m_\Lambda}, \hat{\xi} + \frac{\vec{p}_\Lambda \cdot \hat{\xi}}{m_\Lambda(E_\Lambda + m_\Lambda)} \vec{p}_\Lambda \right). \quad (40)$$

We also introduce 3 orthogonal unit vectors along the longitudinal, transverse, and normal components of  $\Lambda$  polarization in the  $\Lambda_b$  rest frame as

$$\hat{e}_L = \frac{\vec{p}_\Lambda}{|\vec{p}_\Lambda|}, \quad \hat{e}_T = \frac{\vec{p}_+ \times \vec{p}_\Lambda}{|\vec{p}_+ \times \vec{p}_\Lambda|}, \quad \hat{e}_N = \hat{e}_T \times \hat{e}_L, \quad (41)$$

where  $\vec{p}_\Lambda$  and  $\vec{p}_+$  are 3-dimensional vector momenta of the  $\Lambda$  and  $\ell^+$  in the center of mass of the  $\ell^+ \ell^-$  system. With these spin vectors, one can get the polarized differential decay rate for any spin direction  $\hat{\xi}$  along the  $\Lambda$  baryon spin components:

$$\frac{d\Gamma(\hat{\xi})}{d\hat{s}} = \frac{1}{2} \left( \frac{d\Gamma}{d\hat{s}} \right)_0 \left[ 1 + (P_L \hat{e}_L + P_N \hat{e}_N + P_T \hat{e}_T) \cdot \hat{\xi} \right], \quad (42)$$

where  $P_L$ ,  $P_N$ , and  $P_T$  are the longitudinal, normal, and transverse polarizations of  $\Lambda$  baryon, respectively, and  $(d\Gamma/d\hat{s})_0$  is the unpolarized decay width defined in Eq. (37). These polarization asymmetries  $P_i$  ( $i = L, N, T$ ) are obtained from

$$P_i(\hat{s}) = \frac{\frac{d\Gamma}{d\hat{s}}(\hat{\xi} = \hat{e}_i) - \frac{d\Gamma}{d\hat{s}}(\hat{\xi} = -\hat{e}_i)}{\frac{d\Gamma}{d\hat{s}}(\hat{\xi} = \hat{e}_i) + \frac{d\Gamma}{d\hat{s}}(\hat{\xi} = -\hat{e}_i)}, \quad (43)$$

where

$$\begin{aligned}
P_L(\hat{s}) = & \frac{16m_{\Lambda_b}^2 (\lambda(1, r, \hat{s}))^{1/2}}{2(T_0(\hat{s}) + T_2(\hat{s})/3)} \left[ 8m_\ell^2 m_{\Lambda_b} \left( \operatorname{Re}(D_1^* E_3 - D_3^* E_1) + \sqrt{r} \operatorname{Re}(D_1^* D_3 - E_1^* E_3) \right) \right. \\
& - 4m_\ell^2 m_{\Lambda_b}^2 \hat{s} (|D_3|^2 - |E_3|^2) - 4m_{\Lambda_b} (2m_\ell^2 + m_{\Lambda_b}^2 \hat{s}) \operatorname{Re}(A_1^* B_2 - A_2^* B_1) \\
& - \frac{4}{3} m_{\Lambda_b}^3 \hat{s} v_\ell^2 \left( 3 \operatorname{Re}(D_1^* E_2 - D_2^* E_1) + \sqrt{r} \operatorname{Re}(D_1^* D_2 - E_1^* E_2) \right) \\
& - \frac{4}{3} m_{\Lambda_b} \sqrt{r} (6m_\ell^2 + m_{\Lambda_b}^2 \hat{s} v_\ell^2) \operatorname{Re}(A_1^* A_2 - B_1^* B_2) - \frac{2}{3} m_{\Lambda_b}^4 \hat{s} (2 - 2r + \hat{s}) v_\ell^2 (|D_2|^2 - |E_2|^2) \\
& + (4m_\ell^2 + m_{\Lambda_b}^2 (1 - r + \hat{s})) (|A_1|^2 - |B_1|^2) - (4m_\ell^2 - m_{\Lambda_b}^2 (1 - r + \hat{s})) (|D_1|^2 - |E_1|^2) \\
& - \frac{1}{3} m_{\Lambda_b}^2 (1 - r - \hat{s}) v_\ell^2 (|A_1|^2 - |B_1|^2 + |D_1|^2 - |E_1|^2) \\
& \left. - \frac{1}{3} m_{\Lambda_b}^2 \left[ 12m_\ell^2 (1 - r) + m_{\Lambda_b}^2 \hat{s} (3(1 - r + \hat{s}) + v_\ell^2 (1 - r - \hat{s})) \right] (|A_2|^2 - |B_2|^2) \right], \quad (44)
\end{aligned}$$

$$\begin{aligned}
P_N(\hat{s}) = & \frac{8\pi m_{\Lambda_b}^3 v_\ell (\hat{s})^{1/2}}{2(T_0(\hat{s}) + T_2(\hat{s})/3)} \left[ -2m_{\Lambda_b} (1 - r + \hat{s}) \sqrt{r} \operatorname{Re}(A_1^* D_1 + B_1^* E_1) \right. \\
& + 4m_{\Lambda_b}^2 \hat{s} \sqrt{r} \operatorname{Re}(A_1^* E_2 + A_2^* E_1 + B_1^* D_2 + B_2^* D_1) \\
& - 2m_{\Lambda_b}^3 \hat{s} \sqrt{r} (1 - r + \hat{s}) \operatorname{Re}(A_2^* D_2 + B_2^* E_2) \\
& + 2m_{\Lambda_b} (1 - r - \hat{s}) \left( \operatorname{Re}(A_1^* E_1 + B_1^* D_1) + m_{\Lambda_b}^2 \hat{s} \operatorname{Re}(A_2^* E_2 + B_2^* D_2) \right) \\
& \left. - m_{\Lambda_b}^2 ((1 - r)^2 - \hat{s}^2) \operatorname{Re}(A_1^* D_2 + A_2^* D_1 + B_1^* E_2 + B_2^* E_1) \right], \quad (45)
\end{aligned}$$

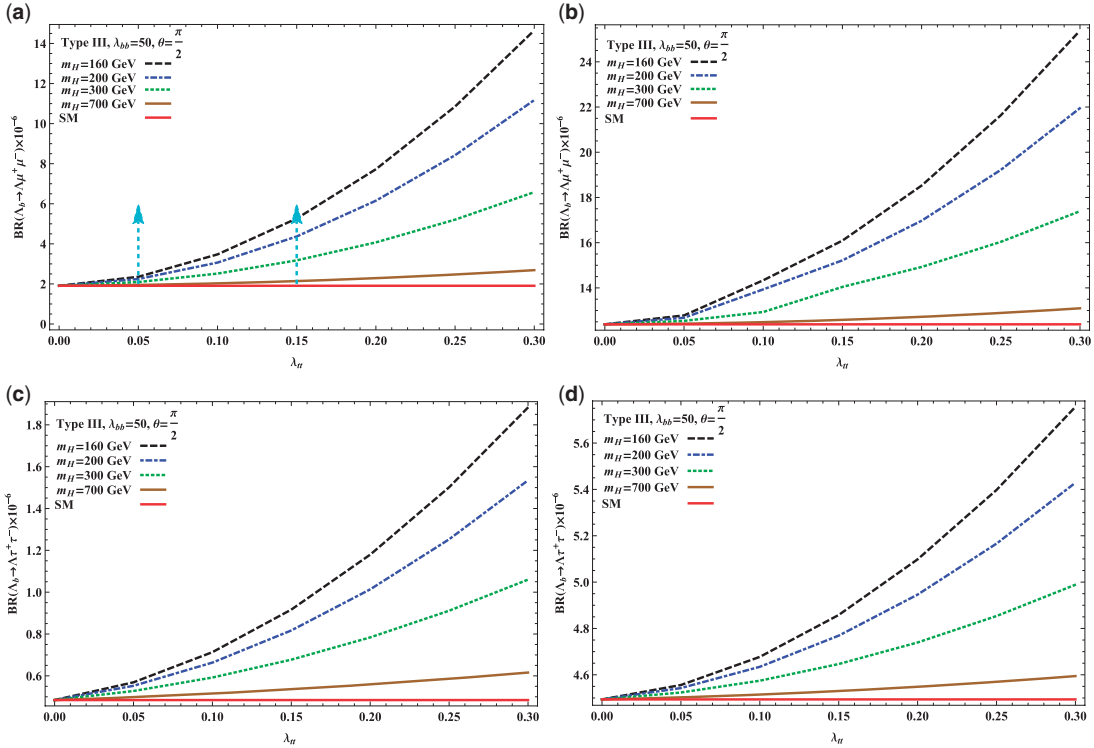
$$\begin{aligned}
P_T(\hat{s}) = & -\frac{8\pi m_{\Lambda_b}^3 v_l (\hat{s} \lambda(1, r, \hat{s}))^{1/2}}{2(T_0(\hat{s}) + T_2(\hat{s})/3)} \left[ m_{\Lambda_b}^2 (1 - r + \hat{s}) \left( \operatorname{Im}(A_2^* D_1 - A_1^* D_2) \right. \right. \\
& - \operatorname{Im}(B_2^* E_1 - B_1^* E_2) \left. \right) + 2m_{\Lambda_b} \left( \operatorname{Im}(A_1^* E_1 - B_1^* D_1) \right. \\
& \left. \left. - m_{\Lambda_b}^2 \hat{s} \operatorname{Im}(A_2^* E_2 - B_2^* D_2) \right) \right]. \quad (46)
\end{aligned}$$

#### 4. Numerical analysis

In this section, we investigate the sensitivity of the branching ratio, differential branching ratio, leptons forward–backward asymmetry, and polarization asymmetries of  $\Lambda$  baryon on the parameters of the 2HDM within the full kinematical interval of the dilepton invariant mass  $4m_\ell^2 \leq q^2 \leq (m_{\Lambda_b} - m_\Lambda)^2$ . The main arbitrary parameters of type III are  $|\lambda_{tt}|$ ,  $|\lambda_{bb}|$ ,  $m_{H^\pm}$ , and the phase angle  $\theta$ . Typically, the  $|\lambda_{tt}|$  and  $|\lambda_{bb}|$  parameters in the Yukawa couplings of type III can be complex,  $\lambda_{tt}\lambda_{bb} = |\lambda_{tt}\lambda_{bb}|e^{i\theta}$ , where the range of variations for  $|\lambda_{tt}|$ ,  $|\lambda_{bb}|$ , and the phase angle  $\theta$  are determined from the experimental results of the electric dipole moments of neutrons,  $B^0 - \overline{B^0}$  mixing,  $R_b \equiv \frac{\Gamma(Z \rightarrow b\bar{b})}{\Gamma(Z \rightarrow \text{hadrons})}$ ,  $\text{Br}(b \rightarrow s\gamma)$ , and  $\rho_0 = \frac{M_W^2}{M_Z^2 \cos^2 \theta}$  (Refs. [44–47]). The physical regions for these parameters have become more controlled as time goes on. The experimental bounds on the neutron electric dipole moments and  $\text{Br}(b \rightarrow s\gamma)$ , as well as  $m_{H^\pm} \geq 160$  GeV, obtained at LEP II constrain  $\lambda_{tt}\lambda_{bb}$  to be less than 1 and  $\theta$  to be in the range  $60^\circ$ – $90^\circ$ . Similarly, the experimental mixing parameter  $x_d = \frac{\Delta M_B}{\Gamma_B}$ ,

**Table 3.** Values of input parameters used in our numerical analysis (Ref. [52]).

$m_{\Lambda_b} = 5.62 \text{ GeV}$ , $m_b = 4.8 \text{ GeV}$ , $m_\mu = 0.105 \text{ GeV}$ ,
$m_\tau = 1.77 \text{ GeV}$ , $ V_{tb} V_{ts}^*  = 45 \times 10^{-3}$ , $m_c = 1.3 \text{ GeV}$ ,
$\alpha^{-1} = 137$ , $G_F = 1.17 \times 10^{-5} \text{ GeV}^{-2}$ ,
$\tau_{\Lambda_b} = 1.383 \times 10^{-12} \text{ s}$ , $m_\Lambda = 1.115 \text{ GeV}$

**Fig. 1.** The central values of branching ratios for the  $\Lambda_b \rightarrow \Lambda \ell^+ \ell^-$  ( $\ell = \mu, \tau$ ) decays as functions of  $\lambda_{tt}$  without long-distance contributions (a,c) and with long-distance contributions (b,d).

$\Delta M_B$  and  $\Gamma_B$  being the mass difference and the average width for the  $B^0$ -meson mass eigenstates, controls  $|\lambda_{tt}|$  to be less than 0.3 (Ref. [34]). Further constraints come from experimental results, like  $BR(B \rightarrow \tau \nu)$ ,  $R(D^*) = \frac{\Gamma(B \rightarrow D^* \mu \nu_\mu)}{\Gamma(B \rightarrow D^* \ell \nu_\ell)}$ , and  $BR(t \rightarrow cg)$  (Ref. [34]). On the other hand, the experimental value of the parameter  $R_b$  constrains the size of  $|\lambda_{bb}|$  to be around 50. (See, e.g., Refs. [34,35], and references therein). From the CLEO data of  $BR(B \rightarrow X_S \gamma)$ , some constraint on  $m_{H^\pm}$  in model III can also be found (Ref. [46]).

The other main input parameters are listed in Tables 2 and 3, while the values of the Wilson coefficients in the SM are presented in Table 1. The obtained numerical results are shown in Figs. 1–5. From the figures it is clear that the long-distance contributions (the charmonium resonances) can give real effects on those observables by taking into account the first two low-lying resonances  $J/\psi$  and  $\psi'$ .

For the sake of convenience, Fig. 1 shows the  $|\lambda_{tt}|$  dependence of the branching ratios  $BR(\Lambda_b \rightarrow \Lambda \ell^+ \ell^-)$  ( $\ell = \mu, \tau$ ) in the SM and the 2HDM of type III for  $|\lambda_{bb}| = 50$ ,  $\theta = 90^\circ$ , and for different values of  $m_{H^\pm}$  with and without LD contributions, respectively. In Fig. 1, we have respected both the upper limit of  $|\lambda_{tt}| \leq 0.3$  and the lower limit of  $m_{H^\pm} \geq 160 \text{ GeV}$  (Refs. [1,34,48]). From Fig. 1,

**Table 4.** The obtained central values of the branching ratios for  $\Lambda_b \rightarrow \Lambda \ell^+ \ell^-$  in both the SM and 2HDM. The experimental branching ratio for  $\Lambda_b \rightarrow \Lambda \mu^+ \mu^-$  in units of  $10^{-6}$  are measured by the CDF BR( $\Lambda_b \rightarrow \Lambda \mu^+ \mu^-$ )= $1.73 \pm 0.42$  (stat)  $\pm 0.55$  (syst) (Ref. [25]), and LHCb BR( $\Lambda_b \rightarrow \Lambda \mu^+ \mu^-$ )= $0.96 \pm 0.16$  (stat)  $\pm 0.13$  (syst)  $\pm 0.21$  (norm) (Ref. [26]) Collaborations, respectively.

Branching ratio $\times 10^{-6}$	$\Lambda_b \rightarrow \Lambda \mu^+ \mu^-$ without LD	$\Lambda_b \rightarrow \Lambda \mu^+ \mu^-$ with LD	$\Lambda_b \rightarrow \Lambda \tau^+ \tau^-$ without LD	$\Lambda_b \rightarrow \Lambda \tau^+ \tau^-$ with LD
SM	1.9	12.38	0.48	4.49
$m_H = 160 \text{ GeV},  \lambda_{tt}  = 0.05$	2.35	12.78	0.57	4.55
$m_H = 160 \text{ GeV},  \lambda_{tt}  = 0.10$	3.47	14.33	0.71	4.67
$m_H = 160 \text{ GeV},  \lambda_{tt}  = 0.15$	5.26	16.09	0.96	4.86
$m_H = 200 \text{ GeV},  \lambda_{tt}  = 0.05$	2.34	12.68	0.55	4.54
$m_H = 200 \text{ GeV},  \lambda_{tt}  = 0.10$	3.06	13.95	0.66	4.63
$m_H = 200 \text{ GeV},  \lambda_{tt}  = 0.15$	4.39	15.21	0.82	4.77
$m_H = 300 \text{ GeV},  \lambda_{tt}  = 0.05$	2.09	12.54	0.52	4.52
$m_H = 300 \text{ GeV},  \lambda_{tt}  = 0.10$	2.51	12.93	0.59	4.57
$m_H = 300 \text{ GeV},  \lambda_{tt}  = 0.15$	3.17	14.04	0.68	4.65
$m_H = 700 \text{ GeV},  \lambda_{tt}  = 0.05$	1.95	12.41	0.49	4.50
$m_H = 700 \text{ GeV},  \lambda_{tt}  = 0.10$	2.02	12.48	0.52	4.51
$m_H = 700 \text{ GeV},  \lambda_{tt}  = 0.15$	2.14	12.58	0.54	4.53

it follows that the new physics contribution of type III 2HDM can offer one maximum 6–7 times enhancement for the branching ratio  $\text{BR}(\Lambda_b \rightarrow \Lambda \mu^+ \mu^-)$  at  $m_{H^\pm} = 160 \text{ GeV}$  and  $|\lambda_{tt}| = 0.3$  (Refs. [25,26]). Furthermore, one can see from Fig. 1(a) that when  $0.05 \leq |\lambda_{tt}| \leq 0.15$  for  $160 \text{ GeV} \leq m_{H^\pm} \leq 300 \text{ GeV}$ , the contribution of type III 2HDM exceeds the SM ones by at most 1–2 times. The numerical values of the branching ratios for  $\Lambda_b \rightarrow \Lambda \ell^+ \ell^- (\ell = \mu, \tau)$  with and without LD contribution in the SM and 2HDM are summarized in Table 4.

Generally speaking, the branching ratios in 2HDM always exceed the SM predictions, and become more important at  $0.05 \leq |\lambda_{tt}| \leq 0.15$  when  $160 \text{ GeV} \leq m_{H^\pm} \leq 300 \text{ GeV}$ . The general behavior of 2HDM contributions is that an increase in the values of  $|\lambda_{tt}|$  creates an increase in the values of the branching ratios, while an increase in the values of  $m_{H^\pm}$  causes a decrease in the values of the branching ratios. For example, when  $m_{H^\pm} = 700 \text{ GeV}$  the branching ratios within 2HDM exceed the SM results slightly, but still agree with a recent CDF measurement  $\text{BR}(\Lambda_b \rightarrow \Lambda \mu^+ \mu^-) = [1.73 \pm 0.42 \text{ (stat)} \pm 0.55 \text{ (syst)}] \times 10^{-6}$  (Ref. [25]), and the LHCb Collaboration  $\text{BR}(\Lambda_b \rightarrow \Lambda \mu^+ \mu^-) = [0.96 \pm 0.16 \text{ (stat)} \pm 0.13 \text{ (syst)} \pm 0.21 \text{ (norm)}] \times 10^{-6}$  (Ref. [26]). Thus, a sensitive measurement of  $\text{BR}(\Lambda_b \rightarrow \Lambda \ell^+ \ell^-) (\ell = \mu, \tau)$ , as well as the value of  $|\lambda_{tt}|$ , will in future play a critical role in establishing new physics beyond the SM, in particular 2HDM.

In Fig. 2, we show the dependence of the differential branching ratios of  $\Lambda_b \rightarrow \Lambda \ell^+ \ell^- (\ell = \mu, \tau)$  on  $q^2$  with and without LD contributions by using the reference values for the parameters as specified before:  $|\lambda_{tt}| = 0.15$ ,  $|\lambda_{bb}| = 50$ , and  $\theta = 90^\circ$ . From Fig. 2, the agreement of the SM with experimental data in the dilepton-invariant mass-squared region  $15 < q^2 < 20 \text{ GeV}^2$  for  $\mu^+ \mu^-$  channel is clear (Ref. [27]). Also, one can see that the 2HDM effects are significant for both muon and tau pairs being in the final state.

In Fig. 3, the leptons  $A_{\text{FB}}$  for  $\Lambda_b \rightarrow \Lambda \ell^+ \ell^- (\ell = \mu, \tau)$  decay as functions of  $q^2$  are presented. Figure 3(a,b) describes the leptons  $A_{\text{FB}}$  in the  $\Lambda_b \rightarrow \Lambda \mu^+ \mu^-$  channel with and without LD contributions, from which one can easily distinguish between the SM and 2HDM. It is clear from the figure that in the SM the zero position of  $A_{\text{FB}}$  is due to the opposite signs of  $C_7^{\text{SM}}(\mu)$  and  $C_9^{\text{SM}}$ , whereas

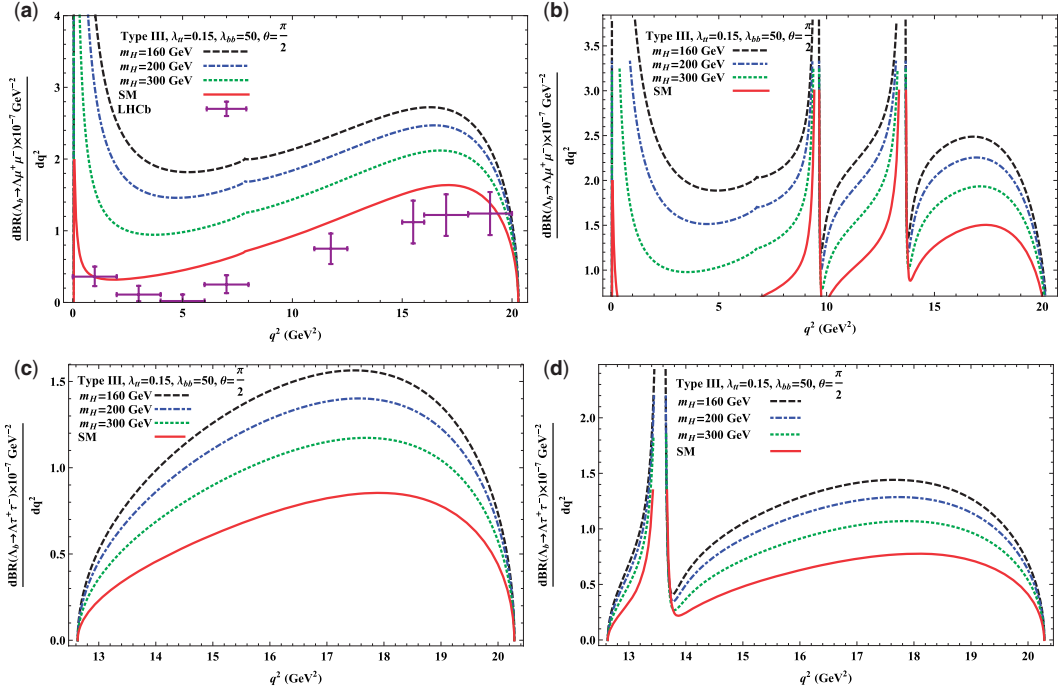


**Fig. 2.** The central values of the differential branching ratios for the  $\Lambda_b \rightarrow \Lambda \ell^+ \ell^-$  ( $\ell = \mu, \tau$ ) decays as functions of  $q^2$  without long-distance contributions (a,c) and with long-distance contributions (b,d). The solid (red), dashed (black), dashed-dot (blue), and dotted (green) lines represent SM,  $m_H=160$  GeV,  $m_H=200$  GeV, and  $m_H=300$  GeV, respectively. The recent experimental result LHCb (Ref. [27]) is also presented in (a).

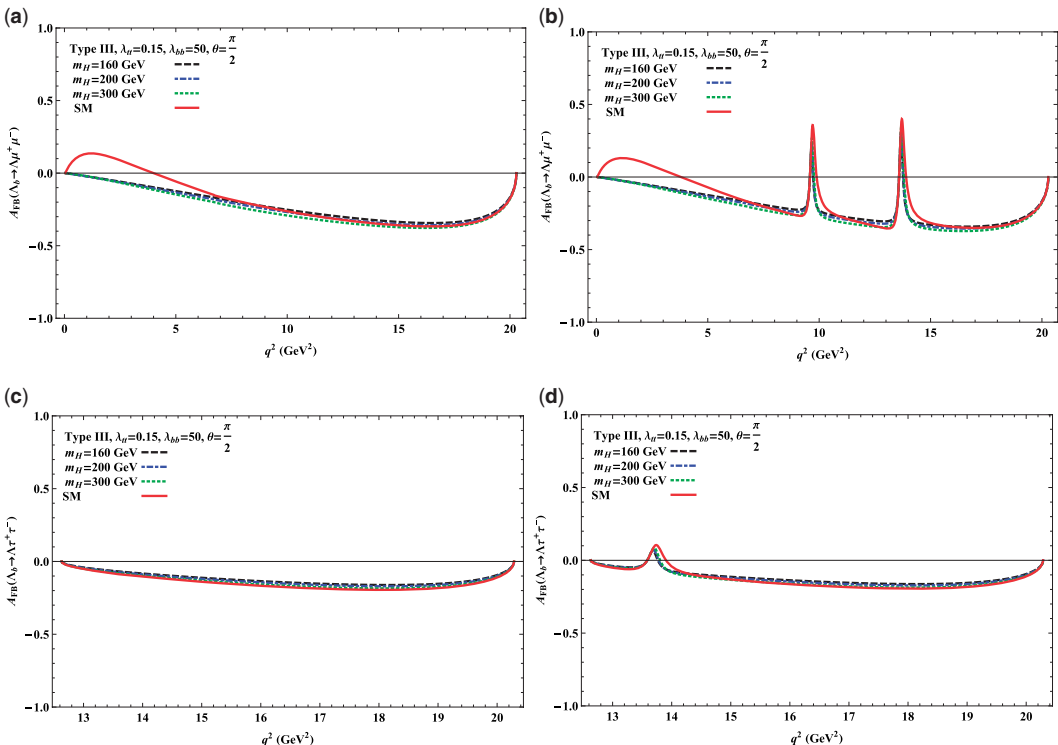


**Fig. 3.** The central values of the leptons forward–backward asymmetry for the  $\Lambda_b \rightarrow \Lambda \ell^+ \ell^-$  ( $\ell = \mu, \tau$ ) decay as functions of  $q^2$  without long-distance contributions (a,c) and with long-distance contributions (b,d). The line conventions are same as given in the legend of Fig. 2.

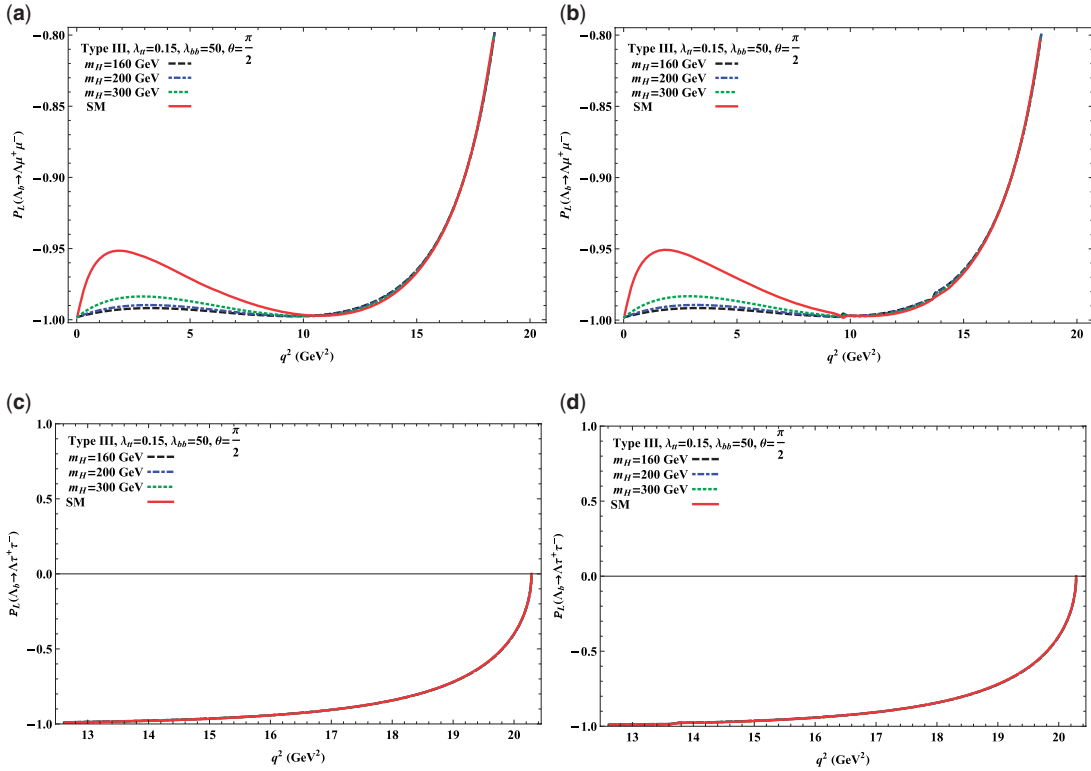


**Fig. 4.** The central values of the longitudinal  $\Lambda$  polarization asymmetries for the  $\Lambda_b \rightarrow \Lambda \ell^+ \ell^-$  ( $\ell = \mu, \tau$ ) decays as functions of  $q^2$  without long-distance contributions (a,c) and with long-distance contributions (b,d). The line conventions are same as given in the legend of Fig. 2.

in 2HDM, the signs of  $C_7^{\text{eff}}(\mu)$  and  $C_9^{\text{eff}}(\mu)$  are the same and have considerable contributions, and hence the zero point of  $A_{\text{FB}}$  completely disappears. Moreover, it should be noted that at  $q^2 \leq 5 \text{ GeV}^2$  the signs of  $A_{\text{FB}}$  in the SM and 2HDM are completely different. Thus, determining the sign of  $A_{\text{FB}}$  in this domain can give unambiguous information about the existence of the charged Higgs particle. This property is considered to be one of the most promising tools in looking for new physics beyond the SM.

For  $\Lambda_b \rightarrow \Lambda \tau^+ \tau^-$  the  $A_{\text{FB}}$  with and without LD contributions are represented in Fig. 3(c,d). For this channel, the  $A_{\text{FB}}$  are found to be insensitive to effects coming from different  $m_{H^\pm}$  masses in the 2HDM, and the 2HDM prediction for  $A_{\text{FB}}$  in the region  $q^2 \simeq 15-17 \text{ GeV}^2$  is slightly smaller than the SM one.

Figure 4 shows the dependence of longitudinal polarization asymmetry of the  $\Lambda$  baryon on the square of momentum transfer. In Fig. 4(a,b), the effects of 2HDM show overall considerable deviations from SM results in the low momentum transfer regions  $0 < q^2 < 5 \text{ GeV}^2$  for the  $\Lambda_b \rightarrow \Lambda \mu^+ \mu^-$  channel, the  $P_L$  asymmetry of the  $\Lambda$  baryon is large and negative in all cases. On the other hand, for the  $\Lambda_b \rightarrow \Lambda \tau^+ \tau^-$  channel in Fig. 4(c,d), the  $P_L$  asymmetry of the  $\Lambda$  baryon in 2HDM is indistinguishable from that in the SM. Therefore, the  $P_L$  asymmetry of the  $\Lambda$  baryon for the muonic mode is predictive for establishing new physics beyond the SM. However, one can easily see that the  $P_N$  asymmetry of the  $\Lambda$  baryon is very sensitive to the sign of the  $C_7^{\text{eff}}(\mu)$  in 2HDM, and its result is also distinguishable from the SM as shown in Fig. 5. The  $P_N$  asymmetry of the  $\Lambda$  baryon is negative in the low momentum transfer regions  $1 < q^2 < 10 \text{ GeV}^2$ , positive and large in the high momentum transfer regions  $10 < q^2 < 20 \text{ GeV}^2$ . In the low region, increasing  $m_{H^\pm}$  decreases the

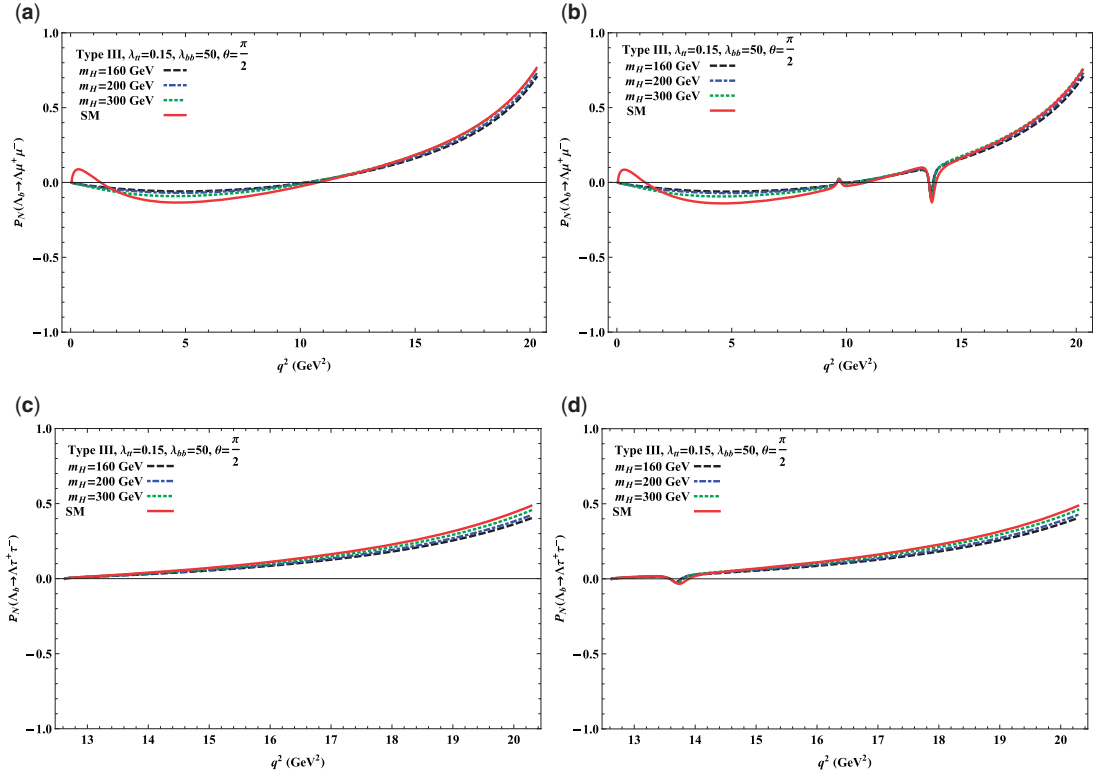


**Fig. 5.** The central values of the normal  $\Lambda$  polarization asymmetries for the  $\Lambda_b \rightarrow \Lambda \ell^+ \ell^-$  ( $\ell = \mu, \tau$ ) decays as functions of  $q^2$  without long-distance contributions (a,c) and with long-distance contributions (b,d). The line conventions are same as given in the legend of Fig. 2.

values of the normal polarization asymmetry. For example, with  $m_{H^\pm} = 160$  GeV the values of  $P_N$  decrease to about 60% of the SM results. Therefore, independent measurements of branching ratios and measurements of longitudinal and normal polarization asymmetries for  $\Lambda_b \rightarrow \Lambda \ell^+ \ell^-$  in future experiments will be a useful tool for establishing the 2HDM.

Finally, from Eq. (46) it is clear that the transverse polarization asymmetry of the  $\Lambda$  baryon is proportional to the imaginary parts of  $C_7^{*\text{eff}}(\mu)$  and  $C_9^{*\text{eff}}(\mu)$ . These imaginary parts are quite small in the 2HDM, as well as in the SM, and hence the values of the transverse polarization asymmetries of the  $\Lambda$  baryon at different values of  $m_{H^\pm}$  and  $|\lambda_{tt}|$  are almost equal to zero. For this reason we do not show them here.

## 5. Conclusion

In this paper, we have carried out a comprehensive analysis on  $\Lambda_b \rightarrow \Lambda \ell^+ \ell^-$  ( $\ell = \mu, \tau$ ) decays in the general 2HDM of type III. We have calculated the branching ratios, differential branching ratios, leptons forward–backward asymmetry, and  $\Lambda$  baryon polarizations using lattice QCD calculations of the relevant  $\Lambda_b \rightarrow \Lambda$  form factors. We have shown that the branching ratios and the differential branching ratios in 2HDM deviate sizably from those of the SM, especially in the large momentum transfer region. For the leptons forward–backward asymmetry in  $\Lambda_b \rightarrow \Lambda \ell^+ \ell^-$  ( $\ell = \mu, \tau$ ) decays the deviations from the SM are very mild in 2HDM. Moreover, in the 2HDM of type III the zero point of the  $A_{FB}$  completely disappears, and the sign predicted in 2HDM is different from that in the SM at  $q^2 \leq 5$  GeV $^2$  in the muon channel. In short, we think that the orders of the obtained values

of the branching ratios, differential branching ratios, leptons  $A_{FB}$ ,  $P_L$ , and  $P_N$  polarizations of the  $\Lambda$  baryon in  $\Lambda_b \rightarrow \Lambda \ell^+ \ell^-$  ( $\ell = \mu, \tau$ ) decays can be measured at the LHCb.

To conclude, even though there are several angular distributions that have already been measured at the LHCb (see, e.g., Ref. [27]), and several updated theoretical discussions on such decay (Refs. [49–51]), still one needs precise measurement of such quantities, like the branching ratio, differential branching ratio, leptons forward–backward asymmetry, and polarization asymmetry of the  $\Lambda$  baryon in  $\Lambda_b \rightarrow \Lambda \ell^+ \ell^-$  ( $\ell = \mu, \tau$ ) decays, which will be helpful in searching for charged Higgs particles, and open the possibility of establishing new physics beyond the SM.

## Funding

Open Access funding: SCOAP<sup>3</sup>.

## References

- [1] G. Aad et al. [ATLAS Collaboration], Phys. Lett. B **716**, 1 (2012).
- [2] S. Chatrchyan et al. [CMS Collaboration], Phys. Lett. B **716**, 30 (2012).
- [3] A. Crivellin, C. Greub, and A. Kokulu, Phys. Rev. D **87**, 094031 (2013).
- [4] S. Chatrchyan et al. [CMS Collaboration], J. High Energy Phys. **06**, 081 (2013).
- [5] T. Enomoto and R. Watanabe, J. High Energy Phys. **05**, 002 (2016).
- [6] G. C. Branco, P. M. Ferreira, L. Lavoura, M. N. Rebelo, M. Sher, and J. P. Silva, Phys. Report **516**, 1 (2012).
- [7] W. Mader, J. H. Park, G. M. Pruna, D. Stöckinger, and A. Straessner, J. High Energy Phys. **09**, 125 (2012); **01**, 006 (2014) [erratum].
- [8] R. Aaij et al. [LHCb Collaboration], Phys. Rev. Lett. **111**, 191801 (2013).
- [9] R. Aaij et al. [LHCb Collaboration], Phys. Rev. Lett. **113**, 151601 (2014).
- [10] R. Aaij et al. [LHCb Collaboration], J. High Energy Phys. **02**, 104 (2016).
- [11] A. Abdesselam et al. [Belle Collaboration], arXiv:1604.04042 [hep-ex] [Search INSPIRE].
- [12] S. Wehle et al. [Belle Collaboration], arXiv:1612.05014 [hep-ex] [Search INSPIRE].
- [13] B. Capdevila, A. Crivellin, S. Descotes-Genon, J. Matias, and J. Virto, arXiv:1704.05340 [hep-ph] [Search INSPIRE].
- [14] W. Altmannshofer, P. Stangl, and D. M. Straub, arXiv:1704.05435 [hep-ph] [Search INSPIRE].
- [15] G. D’Amico, M. Nardecchia, P. Panci, F. Sannino, A. Strumia, R. Torre, and A. Urbano, arXiv:1704.05438 [hep-ph] [Search INSPIRE].
- [16] L. S. Geng, B. Grinstein, S. Jäger, J. M. Camalich, X. L. Ren, and R. X. Shi, arXiv:1704.05446 [hep-ph] [Search INSPIRE].
- [17] G. Hiller and I. Nisandzic, arXiv:1704.05444 [hep-ph] [Search INSPIRE].
- [18] A. Celis, J. Fuentes-Martin, A. Vicente, and J. Virto, arXiv:1704.05672 [hep-ph] [Search INSPIRE].
- [19] A. K. Alok, D. Kumar, J. Kumar, and R. Sharma, arXiv:1704.07347 [hep-ph] [Search INSPIRE].
- [20] A. K. Alok, B. Bhattacharya, A. Datta, D. Kumar, J. Kumar, and D. London, arXiv:1704.07397 [hep-ph] [Search INSPIRE].
- [21] W. Wang, and S. Zhao, arXiv:1704.08168 [hep-ph] [Search INSPIRE].
- [22] T. Mannel and S. Recksiegel, J. Phys. G **24**, 979 (1998).
- [23] T. M. Aliev, A. Ozpineci, and M. Savci, Nucl. Phys. B **709**, 115 (2005).
- [24] Y. M. Wang, M. J. Aslam, and C. D. Lu, Eur. Phys. J. C **59**, 847 (2009).
- [25] T. Aaltonen et al. [CDF Collaboration], Phys. Rev. Lett. **107**, 201802 (2011).
- [26] R. Aaij et al. [LHCb Collaboration], Phys. Lett. B **725**, 25 (2013).
- [27] R. Aaij et al. [LHCb Collaboration], J. High Energy Phys. **06**, 115 (2015) [arXiv:1503.07138 [hep-ex]] [Search INSPIRE].
- [28] T. Barakat, J. Phys. G **24**, 1903 (1998).
- [29] T. Barakat, Il Nuovo Cimento **112**, 697 (1999).
- [30] T. M. Aliev and E. O. Iltan, Phys. Rev. D **58**, 095014 (1998).
- [31] T. M. Aliev and E. O. Iltan, J. Phys. G **25**, 989 (1999).
- [32] B. Grinstein, M. J. Savage, and M. B. Wise, Nucl. Phys. B **319**, 271 (1989).
- [33] Y. B. Dai, C. S. Huang, J. T. Li, and W. J. Li, Phys. Rev. D **67**, 096007 (2003).

- [34] C. S. Kim, Y. W. Yoon, and X. Yuan, J. High Energy Phys. **12**, 038 (2015).
- [35] F. Falahati and R. Khosravi, Phys. Rev. D **85**, 075008 (2012).
- [36] A. J. Buras and M. Münz, Phys. Rev. D **52**, 186 (1995).
- [37] D. Melikhov, N. Nikitin, and S. Simula, Phys. Lett. B **430**, 332 (1998).
- [38] T. M. Aliev, A. Özpineci, and M. Savci, Nucl. Phys. B **649**, 168 (2003).
- [39] C. H. Chen and C. Q. Ceng, Phys. Rev. D **64**, 074001 (2001).
- [40] W. Detmold and S. Meinel, Phys. Rev. D **93**, 074501 (2016).
- [41] Y. M Wang, Y. Li, and C. D Lu, Eur. Phys. J. C **59**, 861 (2009).
- [42] Y. M. Wang and Y. L. Shen, J. High Energy Phys. **02**, 179 (2016).
- [43] T. M. Aliev, K. Azizi, and M. Savci, Phys. Rev. D **81**, 056006 (2010).
- [44] Y. Liu, L. L. Liu, and X. H. Guo, arXiv:1503.06907 [Search INSPIRE].
- [45] D. Atwood, L. Reina, and A. Soni, Phys. Rev. D **55**, 3156 (1997).
- [46] D. Bowser-Chao, K. Cheung, and W. Y. Keung, Phys. Rev. D **59**, 115006 (1999).
- [47] C. S. Huang and S. H. Zhu, Phys. Rev. D **68**, 114020 (2003).
- [48] A. G. Akeroyd et al., Eur. Phys. J. C **77**, 276 (2017).
- [49] S. Meinel and D. V. Dyki, Phys. Rev. D **94**, 013007 (2016).
- [50] G. Kumar and M. Mahajan, arXiv:1511.00935 [Search INSPIRE].
- [51] P. Böer, T. Feldmann, and D. v. Dyk, J. High Energy Phys. **01**, 155 (2015).
- [52] K. Olive et al. [Particle Data Group Collaboration], Chin. Phys. C **38**, 090001 (2014).
- [53] C. B. Lang, D. Mohler, S. Prelovsek, and R. M. Woloshyn, Phys. Lett. B **750**, 17 (2015) [arXiv:1501.01646 [hep-lat]] [Search INSPIRE].